Theoretical calculation of the melting curve of Cu-Zr binary alloys

K. G. S. H. Gunawardana, S. R. Wilson, and M. I. Mendelev
Ames Laboratory, Iowa State University, Ames, Iowa 50011, USA

Xueyu Song*
Ames Laboratory and Department of Chemistry, Iowa State University, Ames, Iowa 50011, USA
(Received 8 September 2014; published 14 November 2014)

Helmholtz free energies of the dominant binary crystalline solids found in the Cu-Zr system at high temperatures close to the melting curve are calculated. Our theoretical approach combines fundamental measure density functional theory (applied to the hard-sphere reference system) and a perturbative approach to include the attractive interactions. The studied crystalline solids are Cu(fcc), $Cu_{51}Zr_{14}(\beta)$, CuZr(B2), $CuZr_2$(C11b), Zr(hcp), and Zr(bcc). The calculated Helmholtz free energies of crystalline solids are in good agreement with results from molecular-dynamics (MD) simulations. Using the same perturbation approach, the liquid phase free energies are calculated as a function of composition and temperature, from which the melting curve of the entire composition range of this system can be obtained. Phase diagrams are determined in this way for two leading embedded atom method potentials, and the results are compared with experimental data. Theoretical melting temperatures are compared both with experimental values and with values obtained directly from MD simulations at several compositions.

DOI: 10.1103/PhysRevE.90.052403 PACS number(s): 68.08.−p, 64.10.+h, 64.75.−g

I. INTRODUCTION

The discovery of bulk metallic glass (BMG) behavior in the Cu-Zr binary system [1,2] has generated great interest as BMG exists in very few binary systems and it has unique tunable mechanical properties [3,4]. However, the formation of BMG in deeply cooled melts and its structural order are still not well understood [4–7]. It is believed that this phenomenon should depend mainly on the kinetics and thermodynamics of accessible phases in the supercooled region. Currently, molecular-dynamics (MD) simulations and experimental studies are widely used in glass-formation studies. Alternatively, a comprehensive theoretical approach with the ability to consistently describe the liquid phase as well as the solid phases would have the potential to provide a deeper understanding of the glass-formation process. In this paper, we present a theoretical approach that can be used to predict the thermodynamic properties of liquid and solid phases near the coexistence region of the Cu-Zr system.

The fundamental measure density functional theory in combination with thermodynamic perturbation theory is used to calculate Helmholtz free energies and hence the melting curve of complex binary crystalline phases. Fundamental measure density functional theory (FMT) is known to provide accurate values of the excess free energy of hard-sphere (HS) systems [8–13]. In the liquid region, the functional yields the Mansoori-Carnahan-Starling-Leland (MCSL) equation of state [14] of HS liquid mixtures in a wide range of densities. For a realistic system, the attractive interaction can be captured using the perturbation theory due to Weeks, Chandler, and Andersen (WCA) [15,16]. It should be noted that similar perturbation approaches in combination with a HS reference system have been used before to calculate the free energies of liquid mixtures and binary alloys [17]. However, these approaches are either based on different methodologies for each phase, rather than on a single theoretical approach, or only for very simple crystalline structures [18]. The approach presented in this paper computes the free energies of all solid and liquid phases within a single theoretical framework, and hence it has the advantage of providing a consistent description of solid and liquid phase coexistence.

Previously, WCA perturbation theory, as refined by Ree *et al.* [19], has been successfully applied to study melting behavior by calculating the free energy of liquids and simple crystalline solids (fcc), interacting with Lennard-Jones potentials, or metallic systems, interacting with embedded-atom method (EAM) or Finnis-Sinclair (FS) potentials [18,20–24]. In Ref. [22], the parameters of the reference HS system were taken from simulations as there is no density functional that can provide reliable thermodynamic properties of HS bcc crystal, whereas in Refs. [23,24] the necessary properties of the HS system were obtained from FMT. An application to the freezing of LJ mixtures [24] has been successful as the obtained spindle and azeotropic-type solid-liquid phase diagrams of LJ mixtures are in good agreement with simulations. A recent study of the freezing of Cu-Au alloys (fcc solid solutions) reproduced experimental melting curves reasonably well using an EAM potential [18]. A self-contained theoretical approach that does not require any input from simulations would have the potential to provide a broader understanding of the thermodynamics of multicomponent systems as simulations or experimental measurements are often not easily accessible.

In this paper, we present an extension of the above theoretical approach to calculate the Helmholtz free energy of complex crystalline metals in which the interatomic interactions are given by EAM potentials. The studied crystalline structures are Cu-fcc, $Cu_{51}Zr_{14}(\beta)$, CuZr(B2), $CuZr_2$(C11b), Zr-bcc, and Zr-hcp. In this work, we present results using two different EAM potentials developed for the Cu-Zr system, namely a potential developed by Mendelev *et al.* (MKOSYP)

*xsong@iastate.edu

[25] and another potential by Sheng *et al.* (CMS) [26]. We show that our theoretical approach has the potential to provide reasonably accurate results in a wide range of temperatures and composition when compared to simulations and experiments [27].

The rest of the paper is organized as follows. After a concise presentation of the theoretical framework in Sec. II, the calculated Helmholtz free energies are compared with available simulation data [28] for the MKOSYP potential. We also discuss the phase stability of the above-mentioned crystalline solids using both EAM potentials near the melting curve. The calculated melting curves are compared with simulation results and the experimental phase diagram. Some concluding remarks are provided to indicate the complimentary roles of the current approach and molecular-dynamics simulations.

II. THEORETICAL METHODOLOGY

In an EAM potential, the total potential energy of the system can be expressed as

$$E_{\text{tot}} = \sum_i F_\alpha\left(\rho_i^e\right) + \frac{1}{2}\sum_{i,j}\phi_{\alpha\beta}(r_{ij}), \tag{1}$$

where ρ_i^e is the total electron density at the site i due to the surrounding atoms, F_α is the embedding energy of an atom in the host electron sea of the metal, and $\phi_{\alpha\beta}(r_{ij})$ is the interaction energy between an atom pair i and j at a distance of r_{ij}. The indices α and β refers to the species type of atoms i and j. The host electron density of site i can be calculated using the electron density functions f using the relation $\rho_i^e = \sum_j f_{\alpha\beta}(r_{ij})$. Thus, there are as many different values for the ρ_i^e as the number of asymmetric sites in the crystal. To reduce the complexity of the notation, we henceforth denote the nth asymmetric site of the species α as α_n.

To carry out perturbation calculations, we first convert the EAM potential to an effective pair potential $[\psi_{\alpha_n\beta}(r_{ij})]$ by performing a Taylor expansion of the embedding energy function around the host electron density of a given site $(\rho^e_{\alpha_n})$ [29]. The resulting so-called effective pair potential can be expressed up to second order as

$$\psi_{\alpha_n\beta}(r_{ij}) = \phi_{\alpha\beta}(r_{ij}) + 2F_\alpha^{'}\left(\rho^e_{\alpha_n}\right) f_{\alpha\beta}(r_{ij}) + F_\alpha^{''}\left(\rho^e_{\alpha_n}\right) f_{\alpha\beta}(r_{ij})^2. \tag{2}$$

It is noted that in general, $\psi_{\alpha_n\beta}(r_{ij}) \neq \psi_{\beta_n\alpha}(r_{ij})$ when $\alpha \neq \beta$. The equality holds only when the two sites have the same symmetry, hence a certain amount of chemical information due to site-dependent electron density is included even at the pair interaction level. In Fig. 1, the effective pair potential corresponding to the MKOSYP potential is plotted both for the pure material and for the CuZr(B2) structure.

Solid lines represent the interactions in the CuZr(B2) structure, while dashed lines represent Cu-Cu interactions in pure Cu-fcc and Zr-Zr interactions in pure Zr-bcc. In the effective pair potential approximation, the total potential energy can be written as

$$E_{\text{tot}} = \sum_{\alpha_n}\left[F_\alpha\left(\rho^e_{\alpha_n}\right) - \rho^e_{\alpha_n} F_\alpha^{'}\left(\rho^e_{\alpha_n}\right)\right]x_{\alpha_n} + \frac{1}{2}\sum_{i,j}\psi_{\alpha_n\beta_n}(r_{ij}), \tag{3}$$

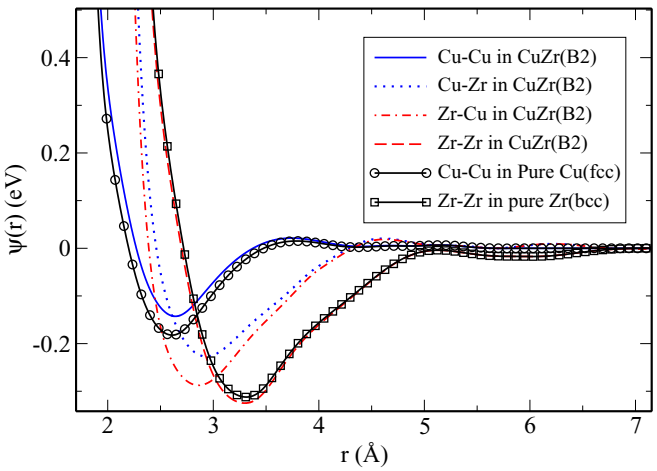

FIG. 1. (Color online) Effective pair potentials for Cu-Cu, Cu-Zr, and Zr-Zr interactions calculated using the MKOSYP potential [25]. The dashed lines represent the Cu-Cu interactions in fcc Cu (black) and Zr-Zr interactions in bcc Zr (blue). Solid lines represent the pair interactions in the CuZr(B2) structure.

where x_{α_n} is the fraction of atoms of type α_n. The summation over α_n is carried out only over the asymmetric sites of both species in a unit cell.

The next step in our calculation is the division of the effective pair potential into a reference and a perturbative potential. We follow the Weeks-Chandler-Anderson (WCA) approach [15,16] to the perturbation theory with some modifications for solid phases. According to the WCA approach, the division point for the reference $(\psi^r_{\alpha_n\beta})$ and the perturbative $(\psi^p_{\alpha_n\beta})$ potentials is set to $r = \lambda_{\alpha_n\beta}$, which is the minimum of the effective pair potential. Thus we write

$$\psi^r_{\alpha_n\beta}(r) = \begin{cases} \psi_{\alpha_n\beta}(r) - \varphi_{\alpha_n\beta}(r), & r \leqslant \lambda_{\alpha_n\beta}, \\ 0, & r > \lambda_{\alpha_n\beta}, \end{cases} \tag{4}$$

$$\psi^p_{\alpha_n\beta}(r) = \begin{cases} \varphi_{\alpha_n\beta}(r), & r \leqslant \lambda_{\alpha_n\beta}, \\ \psi_{\alpha_n\beta}(r), & r > \lambda_{\alpha_n\beta}, \end{cases} \tag{5}$$

where $\varphi = \psi(\lambda) - (r-\lambda)\psi'(r)|_{r=\lambda}$.

Next the reference potential is mapped to an additive HS system with appropriate HS diameters. The HS potential is given by

$$\psi^{\text{HS}}_{\alpha\beta}(r) = \begin{cases} +\infty, & r < d_{\alpha\beta}(T), \\ 0, & r \geqslant d_{\alpha\beta}(T). \end{cases} \tag{6}$$

Effective temperature-dependent HS diameters $[d_{\alpha\beta}(T)]$ in the liquid phase are calculated by numerically solving [30]

$$I_{\alpha\beta} = \int_0^\infty y_{\alpha\beta}(r)\left\{\exp\left[\psi^r_{\alpha\beta}(r)/k_BT\right] - \exp\left[\psi^{\text{HS}}_{\alpha\beta}(r)/k_BT\right]\right\} \times dr = 0, \tag{7}$$

where $y_{\alpha\beta}(r)$ are the cavity functions, k_B is the Boltzmann constant, and T is the temperature. We follow the iterative method described in Ref. [24] instead of solving Eq. (7) directly for the HS diameters of the liquid phase.

For simple closed-packed crystal structures (fcc and hcp), it is reasonable to approximate HS diameters as that of the corresponding liquid [24] due to the similarities in their structures. However, this is not the case when considering complex crystal structures. For complex crystal structures, we found that a first-order approximation to Eq. (7) also yields excellent agreement with the simulation results of crystalline metals. Namely, HS diameters in crystals can be approximated following Barker and Henderson [31] as

$$d^B_{\alpha_n\beta} = \int_0^{\lambda_{\alpha_n\beta}} (1 - e^{-\psi_{\alpha_n\beta}(r)/k_BT})dr. \tag{8}$$

HS diameters of crystalline metals calculated in this manner depend on both temperature and density. This is due to the underlying density dependence of the effective pair potential derived from the EAM potential. An average HS diameter for each species (d_{CuCu} and d_{ZrZr}) is next obtained by averaging over the asymmetric sites of each species:

$$d_{\mathrm{CuCu}} = \frac{1}{N_{\mathrm{Cu}}}\sum_{n=1}^{N_{\mathrm{Cu}}} d^B_{\mathrm{Cu}_n\mathrm{Cu}}, \quad d_{\mathrm{ZrZr}} = \frac{1}{N_{\mathrm{Zr}}}\sum_{n=1}^{N_{\mathrm{Zr}}} d^B_{\mathrm{Zr}_n\mathrm{Zr}}, \tag{9}$$

where N_{Cu} and N_{Zr} are the number of asymmetric sites of Cu and Zr in a given unit cell. The additive condition of HS diameters can be imposed by adjusting the parameters $\lambda_{\alpha_n\beta}$ ($\alpha \neq \beta$) so that $d_{\mathrm{CuZr}} = d_{\mathrm{ZrCu}} = (d_{\mathrm{CuCu}} + d_{\mathrm{ZrZr}})/2$ [24,30].

The resulting mapped HS system may then be treated by methods developed in the context of classical density functional theory (DFT) (see Appendix A). We compute the excess Helmholtz free energy ($F^{\mathrm{ex}}_{\mathrm{HS}}$) using the white-bear version of the fundamental measure theory (FMT) functional [11,13]. For a given atomic packing fraction, $F^{\mathrm{ex}}_{\mathrm{HS}}$ only depends on the diameter ratio defined by $d_{\mathrm{CuCu}}/d_{\mathrm{ZrZr}}$ (<1). The kinetic energy contribution to the free energy of an HS system is accounted for by the ideal gas component:

$$F^{\mathrm{ID}}_{\mathrm{HS}} = \int dr \sum_\alpha \rho(r)x_\alpha\left\{\ln\left[\Lambda^3_\alpha\rho(r)x_\alpha\right] - 1\right\}, \tag{10}$$

where $\rho(r)$ is the density of the solid, $\Lambda_\alpha = h/\sqrt{2\pi m_\alpha k_BT}$ is the de Broglie wavelength of species α, and m is the mass. The integration is carried out over a unit cell of the crystalline solid. The net free energy of the HS system can be written as

$$F_{\mathrm{HS}} = k_BT\left(F^{\mathrm{ex}}_{\mathrm{HS}} + F^{\mathrm{ID}}_{\mathrm{HS}}\right). \tag{11}$$

The contribution of the perturbative potential to the free energy can be calculated using the first-order perturbative correction as follows:

$$F_{\mathrm{PT}} = 2\pi\rho\sum_{\alpha_n,\beta} x_{\alpha_n}x_\beta \int g^{\mathrm{HS}}_{\alpha_n\beta}(r)\psi^p_{\alpha_n\beta}(r)\,r^2\,dr. \tag{12}$$

Within a mean-field approximation, the two-particle distribution function may be written as a product of single-particle density functions, so that $\rho^2(r_1,r_2) = \rho_1(r_1)\rho_2(r_2)$. With this simplification, the radial distribution function of species 2 with respect to species 1 can be expressed as

$$g_{12}(r) = \frac{1}{4\pi V\rho_1\rho_2}\int d\Omega \int d\vec{r}_1\rho_1(\vec{r}_1)\rho_2(\vec{r}_2+\vec{r}). \tag{13}$$

In this approximation, the first peak of the radial distribution function is known to overestimate its true value. Previous work has focused on correcting the pair correlation near the contact radius in simple solids (fcc) [32] and binary solid solutions [33]. These corrections are limited to simple systems, however, and additional complications arise when implemented in complex systems. Thus in this work we are limited to the mean-field pair correlation function. Moreover, we notice that the contribution of such an approximation to the free energy is relatively small. This is due to the flatness of the perturbative potential (according to the WCA) near the contact radius where the deviation of the first peak is larger. Within the density functional formalism, the single-particle density function is described as a summation of Gaussians located at each atomic site, i.e., $\rho_\beta(r) = (\sigma_\beta/\pi)^{3/2}\sum_{R_i} e^{-\sigma_\beta(\vec{r}-\vec{R}_i)}$. Assuming this density profile and fixing the location of the atom at site α_n, it can be shown that

$$g^{\mathrm{HS}}_{\alpha_n\beta}(r) = \frac{1}{4\pi\rho x_\beta r}\left(\frac{\sigma_\beta}{2\pi}\right)^{1/2}\sum_{R_i}\frac{e^{-\sigma_\beta(r-R_i)^2/2} - e^{-\sigma_\beta(r+R_i)^2/2}}{R_i}. \tag{14}$$

The net Helmholtz free energy of the crystalline solid is given by a summation of three components as

$$F(T,\rho) = F_{1\ \mathrm{body}} + F_{\mathrm{HS}} + F_{\mathrm{PT}}, \tag{15}$$

where $F_{1\ \mathrm{body}}(\rho) = \sum_{\alpha_n}[F_\alpha(\rho^e_{\alpha_n}) - \rho^e_{\alpha_n}F'_\alpha(\rho^e_{\alpha_n})]x_{\alpha_n}$ is the one-body term, which is the first part on the right-hand side of Eq. (3).

III. RESULTS

The DFT calculation was carried out in dimensionless units in which the length is scaled by the HS diameter of the larger species (in this case Zr) and the energy is measured in units of k_BT. Having mapped the reference potential into an HS system, we can define atomic packing fractions as $\eta = \pi/6\,\rho(x_{\mathrm{Cu}}d^3_{\mathrm{CuCu}} + x_{\mathrm{Zr}}d^3_{\mathrm{ZrZr}})$, which is useful in distinguishing between the solid and liquid phases. We have previously used the FMT functional to calculate the free energy of binary HS crystals [34]. The calculated excess free energy of AB_{13}, AB_2, and AB-like structures is in good agreement with the results from simulations. For the Cu-Zr system, we studied the HS models of five binary crystals: Cu_5Zr(C15b), $Cu_{51}Zr_{14}(\beta)$, $Cu_{10}Zr_7(\phi)$, CuZr(B2), and $CuZr_2$ (C11b). The fundamental measure functional gives well-behaved minima for four HS crystal complexes in the two-dimensional Gaussian space clearly representing a solid phase. However, we noted that the FMT functional fails to give a stable minimum for the structure $Cu_{10}Zr_7(\phi)$. (More details on the HS calculation can be found in our companion paper [34].) Therefore, in this work we continue with perturbation calculations only for three binary crystals, namely $Cu_{51}Zr_{14}(\beta)$, CuZr(B2), and $CuZr_2$(C11b), as these three binary crystals together with the pure Cu-fcc and Zr-bcc cover more than 90% of the melting curve for this system.

For completeness, we also studied the pure Zr bcc structure following our perturbative approach. However, anomalous behavior of the HS bcc structure using the DFT prevents us from obtaining Gaussian parameters or HS free energies,

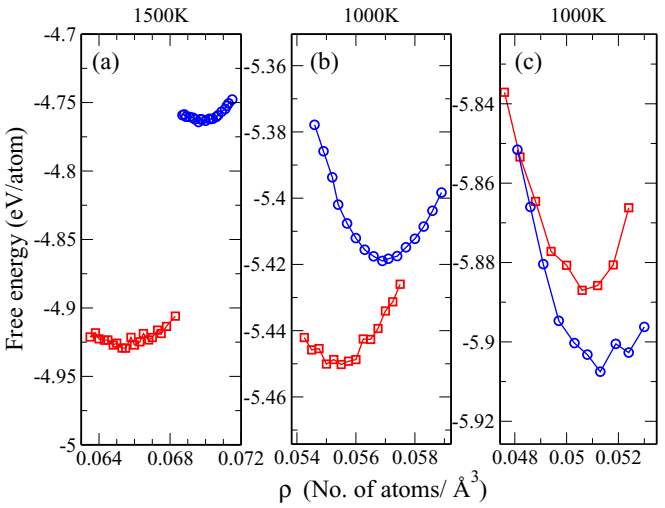

FIG. 2. (Color online) The Helmholtz free energy $F(T,\rho)$ plotted as a function of atomic number density ($\rho = N/V$) for three binary crystals in the Cu-Zr system: (a) $Cu_{51}Zr_{14}$, (b) CuZr, and (c) $CuZr_2$. The minimum of each curve corresponds to the relaxed structure at that temperature. Connected blue circles represent results for the MKOSYP potential, and connected red squares represent the results for the CMS potential.

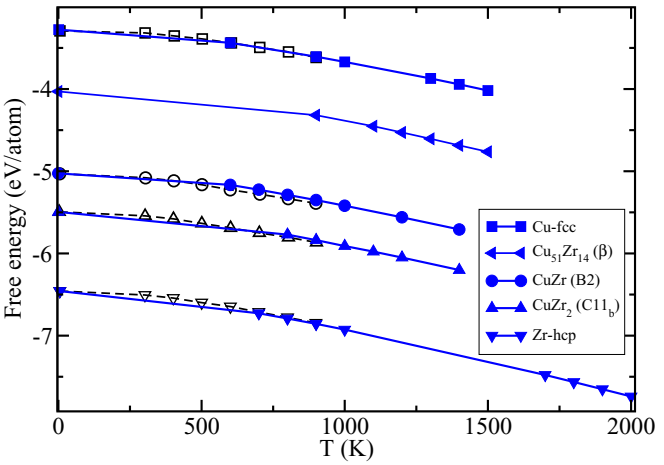

FIG. 3. (Color online) Comparison between the theoretically calculated Helmholtz free energy, F (eV/atom), and the MD simulation. The filled symbols connected by solid lines are from our perturbation calculations using the MKOSYP potential. The open symbols connected by dashed lines refer to MD simulation results using the same EAM potential [28].

in contrast to previous reports [35–37]. Therefore, in our calculations both the Gaussian parameters and the free energies were obtained from simulation results [38].

Given a thermodynamically stable HS reference system, we can perform the perturbation calculations. The Helmholtz free energy is a function of both temperature and atomic density [Eq. (15)]. At a given temperature, we minimized $F(\rho,T)$ to obtain the relaxed structures. The minimization was carried out at finite temperatures by only permitting the lattice constants (a, b, and c) to vary; a full minimization of the structure was only done at 0 K. All finite-temperature calculations are done so as to preserve the lattice symmetry of the structures. For the CuZr, Cu-fcc, and Zr-bcc structures, we set $a = b = c$. For the other structures, aspect ratios were initially set to the following values: for $Cu_{51}Zr_{14}$, $a = b$ and $c/a = 0.7355$; for $CuZr_2$, $a = b$ and $c/a = 3.472$; and for Zr-hcp, $a = b$ and $c/a = 1.6211$. We found that the optimal aspect ratios are very close to the above set values with negligible correction to the free energy. With the above constraints, the minimization is carried out only as a function of the atomic number density $\rho_s = N/V$, where N is the number of atoms in a unit cell and V is the volume. In Fig. 2, the Helmholtz free energy is plotted as a function of number density ρ_s for all three binary crystals studied. The two curves for each structure correspond to the two EAM potentials considered in this calculation. For all structures, we observe a minimum slightly below the experimentally reported number density (see Table I). In Table I, we tabulate the number densities of the relaxed structures calculated at $T = 1200$ K using the MKOSYP potential. For pure Zr (hcp and bcc) crystals, the densities were measured at $T = 1800$ K.

For all crystal structures, the relaxed structure was determined at packing fractions $\eta > 0.54$ and at temperatures below the targeted melting values (see Table I). The variation of η with crystal composition of Zr shows a reciprocal effect to the number density toward the glass-forming region. More precisely, we observed that the atoms in CuZr and $CuZr_2$ are more closely packed compare to the other monatomic crystals, and we also the studied $Cu_{51}Zr_{14}$ structure. This can be attributed to the contrast of the diameter ratio, about 0.79, for this binary system.

In Fig. 3, the Helmholtz free energy is plotted as a function of temperature. The filled symbols are calculated from the

TABLE I. Optimized structure parameters and the predicted melting temperatures compared with experimental data and molecular-dynamics simulations. The number density ρ_s (in units of Å^{-3}) and packing fraction η are given for conditions that minimize $F(\rho,T)$ at 1200 K except for pure Zr. Data for Zr- (bcc and hcp) are taken at 1800 K. The theory and the MD simulation data in this table were produced only using the MKOSYP potential.

Crystal	ρ_s (Theory)	η_s (Theory)	ρ_s (Expt.)	T_m (Theory) (K)	T_m (MD) (K)	T_m (Expt.) (K)
Cu(fcc)	0.0840	0.548	0.0850	1260	1355	1360
$Cu_{51}Zr_{14}(\beta)$	0.0695	0.554	0.0716 [39]	810	1050	1375
CuZr(B2)	0.0574	0.595	0.0577 [40]	1204	1327	1210
$CuZr_2$(C11b)	0.0513	0.605	0.0518 [41]	1060		1276
Zr(bcc)	0.0430	0.560		1891	2100	2125
Zr(hcp)	0.0435	0.568		2090	2110	

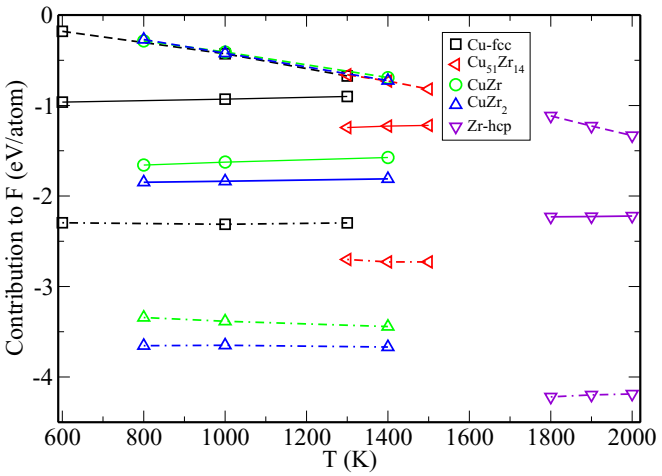

FIG. 4. (Color online) Contributions to the Helmholtz free energy from the HS reference system (dashed lines), the perturbative correction (solid lines), and the one-body term (dotted dashed line) determined by Eq. (15) as a function of temperature.

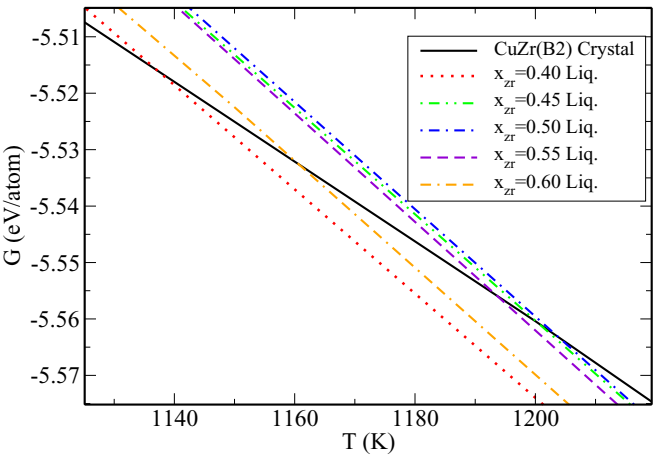

FIG. 5. (Color online) Gibbs free energy at zero pressure for crystalline CuZr (B2) (dashed line) and the left-hand side of Eq. (16) for the liquid mixture (solid lines). The crossing points of the above two lines give the coexistence temperature at the corresponding x_{Zr}.

present theoretical approach using the MKOSYP potential, and open symbols are results obtained in Ref. [28] from molecular-dynamics simulations using the same potential in which the Einstein crystal is taken as a reference system. For one-component crystals (Cu-fcc and Zr-hcp), the agreement between the two calculations is excellent. For CuZr and $CuZr_2$, the difference between the results is about 1% and 0.5%, respectively. However, inaccuracy on the order of 1% could be crucial when determining the melting temperature. The effect on the melting temperature can be minimized by treating the liquid in the same theoretical framework. To do so, we utilize the empirical Mansoori-Carnahan-Starling-Leland (MCSL) equation of state [14], which is the liquid limit of the FMT functional, to treat HS liquid mixtures. The liquid phase calculation was carried out in a similar manner to the procedure described in Refs. [18,24].

More insight into the free energy and its temperature dependence can be obtained by analyzing the behavior of the three contributions to the excess free energy [see Eq. (15)]. Figure 4 shows the relative contribution of the HS reference system (circles), the perturbative terms (triangles), and the one-body terms (squares) to the total free energy, as a function of temperature. For the six crystal structures studied in this work, similar behavior was observed in these three contributions as functions of the density and temperature. The one-body term $F_{1\ \mathrm{body}}(\rho)$ comprises about 60% of the free energy and decreases with increasing ρ_s. The perturbative correction (F_{PT}) accounts for the second-largest contribution to the free energy, and it increases with increasing ρ_s. The smallest contribution is associated with the HS reference system. For most of the structures studied, this contribution comprises about 10% of the total, whereas that of F_{PT} is about 30%. Nonetheless, it is clear that the contribution from the HS reference system contributes substantially to the overall temperature dependence, and therefore an accurate determination of this term is important. In the context of the perturbation approach, the HS reference contribution provides the entropic contribution to the free energy, and hence varies strongly with temperature.

The coexistence temperatures of single-species solids (Cu and Zr) with a liquid mixture of $Cu_{(1-x_l)}Zr_{x_l}$ can be determined by matching the chemical potentials in two phases at zero pressure. The coexistence of binary crystals with a liquid mixture can be obtained by imposing the following equilibrium condition:

$$\left(\mu^L_{\mathrm{Cu}} + n\mu^L_{\mathrm{Zr}}\right)/(1+n) = G^{\mathrm{crystal}}_{\mathrm{Cu}_{1-n}\mathrm{Zr}_n}, \tag{16}$$

where μ^L_{Cu} and μ^L_{Zr} are the chemical potential of Cu and Zr in a liquid of composition x_l. We carried out the matching graphically as illustrated in Fig. 5. The dashed line represents the Gibbs free energy [right-hand side of Eq. (16)] of the CuZr(B2) structure. The solid lines represent the left-hand side of Eq. (16) at different liquid compositions (x_l). The crossing points of these two lines give the melting temperature. It should be noted that the slopes of these two curves are so close that a small discrepancy of the free energy would result in a considerable deviation of the melting temperatures. As a rough estimate, about 1% discrepancy in the free energy would change the melting temperature by 10% of its predicted value.

The above procedure was extended to other crystal structures to trace out the melting curve as depicted in Fig. 6. Both potentials reproduce well the variation of the melting curve for CuZr(B2) structure as a function of x_{Zr}. With increasing Zr concentration in the liquid near $x_{\mathrm{Zr}} \approx 0.66$, $CuZr_2$ structure appears as a stable phase. However, the melting curve lies about 170 K below the experimental prediction. Upon further increasing x_{Zr} above 0.74, we notice that the Zr(bcc) phase stabilizes but with relatively low melting temperature. This behavior qualitatively matches the high-temperature variation of the melting curve of the Cu-Zr system. On the Cu-rich side of the phase diagram, $Cu_{51}Zr_{14}$ is the dominant structure, giving a peak at $T = 1390$ K and $x_{\mathrm{Zr}} = 0.2154$. However, both potentials provide a low melting temperature for this structure (open left triangles connected by a thin dashed line in Fig. 6).

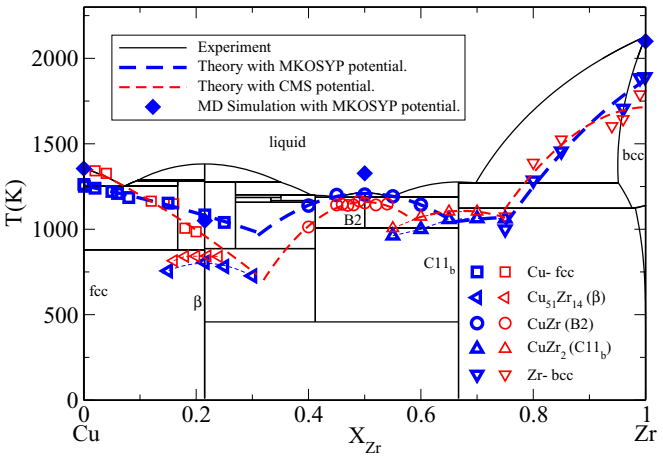

FIG. 6. (Color online) Melting curve (liquidus) predicted from the two EAM potentials (dashed line) compared with the experiment (solid lines) [27]. The filled diamonds represent the melting temperature obtained from the MD simulations.

To gain further understanding of the melting curve, we carried out MD simulations with the MKOSYP potential. For Cu-fcc and Zr-bcc, melting temperatures are about 1355 and 2100 K, respectively. These are almost the same as the experimental values. The melting temperature of CuZr(B2) determined from MD simulations is about 1330 K, which overestimates the experimental value of 1200 K. In general, the discrepancy of our theoretical prediction is less than 10% below the simulated melting temperature on the above three points. In supporting our theoretical prediction, the simulated melting temperature of $Cu_{51}Zr_{14}$, 1050 K is considerably lower than the experimental value (1390 K). The theoretical prediction is about 810 K at $x_{Zr} = 0.2154$.

IV. DISCUSSION AND CONCLUSIONS

Calculating the melting curve from simulations is a computationally intensive task. In particular, to obtain the melting curve for a liquid composition that is different from the solid one using simulations is especially challenging. Furthermore, simulations of supercooled liquid phases present additional challenges. For these situations, applying a free-energy route based upon reliable theoretical methods to estimate the melting curve has several advantages. In this work, we demonstrate that the DFT approach using a recently developed FMT functional in combination with perturbation theory can be successfully applied to binary systems with complex solid phases. The calculated Helmholtz free energies and melting curves of three dominating binary crystals ($Cu_{51}Zr_{14}$, CuZr, $CuZr_2$) and three monatomic crystals [Cu(fcc), Zr(hcp), and Zr(bcc)] validate the current approach.

The agreement between simulation results and the experimental phase diagram is promising. The projected error in the free energy is less than 1% for binary crystals and negligible for monatomic crystals (Cu-fcc and Zr-hcp) when compared with simulations. Nonetheless, even greater precision is required to estimate the melting temperature with precision. Given the above uncertainty in the free-energy calculations, 10–20% discrepancy is possible between simulated and theoretical values for the melting temperature. Comparison between theoretical melting points and values obtained directly from MD simulation confirms the importance of greater precision needed for theoretical calculations of free energies.

The majority of the error in the free energy when computed following this approach is likely associated with the one-body term [see Eq. (15)] since it comprises about 60% of the total. Error in this contribution would probably arise as a result of the procedure required to map the EAM potential to an effective pair potential. Error due to the HS contribution would contribute disproportionately to the variation in the free energy with temperature. In the case considered in this work, the contribution to the total free energy is small (12%). The second largest contribution to the free energy, comprising about 30% of the total, is associated with the perturbative correction. An improved approach to treat the attractive interaction will be essential to improve the overall accuracy of this method.

The low melting temperature for $Cu_{51}Zr_{14}$ obtained in this work could be an artifact of the EAM potential. These potentials are developed to match experimental properties only in a certain window around the glass-forming compositions, with $x_{Zr} \approx 0.5$, and $Cu_{51}Zr_{14}$ evidently falls outside of this window. However, the theoretical approach presented here may apply equally well to interaction potentials based on direct quantum-mechanical computations, and this direction will be the subject of future research.

ACKNOWLEDGMENTS

This research was sponsored by the Division of Materials Sciences and Engineering, Office of Basic Energy Sciences, U.S. Department of Energy, under Contract No. W-7405-ENG-82 with Iowa State University. We would like to thank Shihuai Zhou for providing much of the structural information used in this study.

APPENDIX: FUNDAMENTAL MEASURE THEORY

The density functional theory for many-body classical systems follows the Mermin theorem. Given the grand-canonical ensemble, there exists a functional of single-particle density distributions $\rho_i(\vec{r})$ such that

$$\Omega[\rho_1,\rho_2,\ldots,\rho_\nu] = F[\rho_1,\rho_2,\ldots,\rho_\nu] + \sum_{i=1}^{\nu}\int d^3r\rho_i(\vec{r})\left[V_i^{\text{ext}}(\vec{r}) - \mu_i\right], \quad \text{(A1)}$$

where $V_i^{\text{ext}}(\vec{r})$ is the external potential and μ_i is the chemical potential of species i. The functional describing the Helmholtz free energy $F[\rho_1,\rho_2,\ldots,\rho_\nu]$ is independent of the external potential. The equilibrium density distributions $\rho_i^0(\vec{r})$ and the grand potential can be obtained by the variational principle,

$$\left.\frac{\delta\Omega[\rho_1,\rho_2,\ldots,\rho_\nu]}{\delta\rho_i}\right|_{(\rho_i(\vec{r})=\rho_i^0(\vec{r}))} = 0. \quad \text{(A2)}$$

When studying a crystalline phase, the density profile is assumed to be of a Gaussian form centered at each lattice site. The density profile of species i in a multicomponent system

can be expressed as

$$\rho_i(\vec{r}) = \left(\frac{\alpha_i}{\pi}\right)^{3/2} \sum_{\vec{r}_i} e^{-\alpha_i(\vec{r}-\vec{r}_i)^2}, \tag{A3}$$

where α is the Gaussian parameter and $\vec{r}_i$ is the location of species i. The summation covers all the sites occupied by species i. The system is scaled with respect to the diameter of the largest species (d_A), and the diameter ratio is defined as $\sigma = d_B/d_A$. Then the minimization of the free-energy functional is performed with respect to the dimensionless Gaussian parameters, $\alpha_i d_A^2$.

The Helmholtz free-energy functional of a mixture of ν species can be split into two parts:

$$\beta F[\rho_1,\rho_2,\ldots,\rho_\nu] = \sum_{i=1}^{\nu} \int d^3\vec{r}\left\{\ln\left[\rho_i(\vec{r})\Lambda_i^3\right] - 1\right\}\rho_i(\vec{r}) + \beta F_{\rm ex}[\rho_1,\rho_2,\ldots,\rho_\nu], \tag{A4}$$

where Λ_i is the de Broglie wavelength of species i, and $\beta = 1/k_BT$. The first part on the right-hand side of the above equation gives the contribution due to the noninteracting particles, and the latter is the excess free energy.

In the fundamental measure theory, the hard-sphere interaction contribution to the excess free-energy functional can be expressed in terms of weighted densities as [8,9]

$$\beta F_{\rm ex}[\{\rho_i\}] = \int d^3\vec{r}' \sum_{j=1}^{3} \Phi_j(\eta(\vec{r}),n_i(\vec{r}),\vec{v}_i(\vec{r}),\mathcal{T}_i(\vec{r})), \tag{A5}$$

where the 2 scalar [$\eta_i(\vec{r})$ and $n_i(\vec{r})$], vector [$v_i(\vec{r})$], and tensor [$\mathcal{T}_i(\vec{r})$] weighted densities [12,13] are defined as follows:

$$\eta(\vec{r}) = \sum_{i=1}^{\nu} \int d^3\vec{r}'\rho_i(\vec{r}')\Theta(R_i - |\vec{r}-\vec{r}'|), \tag{A6}$$

$$n_i(\vec{r}) = \frac{1}{4\pi R_i^2} \int d^3\vec{r}'\rho_i(\vec{r}')\delta(R_i - |\vec{r}-\vec{r}'|), \tag{A7}$$

$$\vec{v}_i(\vec{r}) = \frac{1}{4\pi R_i^2} \int d^3\vec{r}'\rho_i(\vec{r}')\delta(R_i - |\vec{r}-\vec{r}'|)\frac{(\vec{r}-\vec{r}')}{R_i}, \tag{A8}$$

$$\mathcal{T}_i^{m,n}(\vec{r}) = \frac{1}{4\pi R_i^2} \int d^3\vec{r}'\rho_i(\vec{r}')\delta(R_i - |\vec{r}-\vec{r}'|) \times \frac{(\vec{r}-\vec{r}')_m(\vec{r}-\vec{r}')_n}{R_i^2}, \tag{A9}$$

where $\mathcal{T}_i^{m,n}(\vec{r})$ ($m,n = 1,2,3$) are the tensor components. The function $\Theta(x)$ is the Heavyside step function and $\delta(x)$ is Dirac's delta function. The R_i is the hard-sphere radius of species i. In the WB version of FMT, the functionals Φ_i are

$$\Phi_1[\rho] = -\int d^3\vec{r}\,\ln[1-\eta(\vec{r})]\sum_{i=1}^{\nu} n_i(\vec{r}), \tag{A10}$$

$$\Phi_2[\rho] = 2\pi \sum_{i,j=1}^{\nu} R_iR_j(R_i+R_j) \times \int d^3\vec{r}\frac{n_i(\vec{r})n_j(\vec{r}) - \vec{v}_i(\vec{r})\cdot\vec{v}_j(\vec{r})}{[1-\eta(\vec{r})]}, \tag{A11}$$

and

$$\Phi_3[\rho] = 12\pi^2 \sum_{i,j,k=1}^{\nu} R_i^2R_j^2R_k^2 \int d^3\vec{r}\varphi_{ijk}(\vec{r})f_3[\eta(\vec{r})], \tag{A12}$$

where

$$\varphi_{ijk}(\vec{r}) = \vec{v}_i\cdot\mathcal{T}_j\cdot\vec{v}_k - n_j\vec{v}_i\cdot\vec{v}_k - {\rm Tr}[\mathcal{T}_i\mathcal{T}_j\mathcal{T}_k] + n_j{\rm Tr}[\mathcal{T}_i\mathcal{T}_k] \tag{A13}$$

and

$$f_3(\eta) = \frac{2}{3\eta}\left(\frac{\eta}{(1-\eta)^2} + \ln(1-\eta)\right). \tag{A14}$$

[1] D. Wang, Y. Li, B. B. Sun, M. L. Sui, K. Lu, and E. Ma, Appl. Phys. Lett. **84**, 4029 (2004).
[2] A. Inoue and W. Zhang, Mater. Trans. **45**, 584 (2004).
[3] M. Chen, Annu. Rev. Mater. Res. **38**, 445 (2008).
[4] W. H. Wang, C. Dong, and C. H. Shek, Mater. Sci. Eng.: R **44**, 45 (2004).
[5] W. Johnson, J. Miner. Met. Mater. **54**, 40 (2002).
[6] A. Inoue, Acta Mater. **48**, 279 (2000).
[7] Y. Q. Cheng, H. W. Sheng, and E. Ma, Phys. Rev. B **78**, 014207 (2008).
[8] Y. Rosenfeld, Phys. Rev. Lett. **63**, 980 (1989).
[9] Y. Rosenfeld, J. Chem. Phys. **93**, 4305 (1990).
[10] Y. Rosenfeld, M. Schmidt, H. Löwen, and P. Tarazona, Phys. Rev. E **55**, 4245 (1997).
[11] P. Tarazona, Phys. Rev. Lett. **84**, 694 (2000).
[12] P. Tarazona, Physica A **306**, 243 (2002).
[13] R. Roth, R. Evans, A. Lang, and G. Kahl, J. Phys.: Condens. Matter **14**, 12063 (2002).
[14] G. A. Mansoori, N. F. Carnahan, K. E. Starling, and J. T. W. Leland, J. Chem. Phys. **54**, 1523 (1971).
[15] J. D. Weeks, D. Chandler, and H. C. Andersen, J. Chem. Phys. **54**, 5237 (1971).
[16] H. C. Andersen, J. D. Weeks, and D. Chandler, Phys. Rev. A **4**, 1597 (1971).
[17] A. Denton, G. Kahl, and J. Hafner, J. Non-Cryst. Solids **250-252**, 15 (1999).
[18] V. B. Warshavsky and X. Song, Phys. Rev. B **79**, 014101 (2009).
[19] H. S. Kang, C. S. Lee, T. Ree, and F. H. Ree, J. Chem. Phys. **82**, 414 (1985).
[20] J. F. Lutsko and G. Nicolis, Phys. Rev. Lett. **96**, 046102 (2006).
[21] C. Rascón, L. Mederos, and G. Navascués, Phys. Rev. Lett. **77**, 2249 (1996).
[22] X. Song and J. R. Morris, Phys. Rev. B **67**, 092203 (2003).
[23] V. B. Warshavsky and X. Song, Phys. Rev. E **69**, 061113 (2004).
[24] V. B. Warshavsky and X. Song, J. Chem. Phys. **129**, 034506 (2008).
[25] M. Mendelev, M. Kramer, R. Ott, D. Sordelet, D. Yagodin, and P. Popel, Philos. Mag. **89**, 967 (2009).
[26] Y. Q. Cheng, E. Ma, and H. W. Sheng, Phys. Rev. Lett. **102**, 245501 (2009).

[27] S. Zhou and R. Napolitano, Acta Mater. **58**, 2186 (2010).
[28] C. Tang and P. Harrowell, J. Phys.: Condens. Matter **24**, 245102 (2012).
[29] S. M. Foiles, Phys. Rev. B **32**, 3409 (1985).
[30] G. Kahl and J. Hafner, J. Phys. F **15**, 1627 (1985).
[31] D. Henderson and J. A. Barker, Phys. Rev. A **1**, 1266 (1970).
[32] C. Rascón, L. Mederos, and G. Navascués, Phys. Rev. E **54**, 1261 (1996).
[33] V. B. Warshavsky and X. Song, Phys. Rev. E **77**, 051106 (2008).
[34] K. G. S. H. Gunawardana and X. Song, J. Phys. Chem. (unpublished).
[35] W. A. Curtin and K. Runge, Phys. Rev. A **35**, 4755 (1987).
[36] J. F. Lutsko and M. Baus, Phys. Rev. A **41**, 6647 (1990).
[37] J. F. Lutsko, Phys. Rev. E **74**, 021121 (2006).
[38] V. B. Warshavsky and X. Song, Phys. Rev. E **86**, 031602 (2012).
[39] J.-P. Gabathuler, P. White, and E. Parthé, Acta Crystallogr. Sect. B **31**, 608 (1975).
[40] E. Carvalho and I. Harris, J. Mater. Sci. **15**, 1224 (1980).
[41] M. V. Nevitt and J. Downey, Trans. TMS-AIME **224**, 195 (1962).